

Constructing a Catalytic Cycle for C–F to C–X (X = O, S, N) Bond Transformation Based on Gold-Mediated Ligand Nucleophilic Attack

Ji-Yun Hu,[†] Jing Zhang,[‡] Gao-Xiang Wang,[†] Hao-Ling Sun,^{*,§} and Jun-Long Zhang^{*,†}

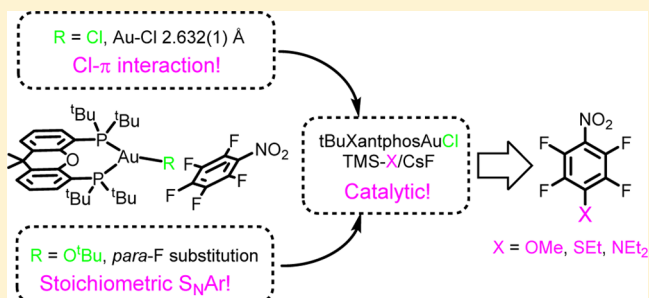
[†]Beijing National Laboratory for Molecular Sciences, State Key Laboratory of Rare Earth Materials Chemistry and Applications, College of Chemistry and Molecular Engineering, Peking University, Beijing 100871, P. R. China

[‡]College of Materials Science and Optoelectronics Technology, Graduate University of Chinese Academy of Sciences, Beijing 100049, P. R. China

[§]Department of Chemistry and Beijing Key Laboratory of Energy Conversion and Storage Materials, Beijing Normal University, Beijing 100875, P. R. China

Supporting Information

ABSTRACT: A tricoordinated gold(I) chloride complex, tBuXantphosAuCl, supported by a sterically bulky 9,9-dimethyl-4,5-bis(di-*tert*-butylphosphino)xanthene ligand (tBuXantphos) was synthesized. This complex features a remarkably longer Au–Cl bond length [2.632(1) Å] than bicoordinated linear gold complexes (2.27–2.30 Å) and tricoordinated XantphosAuCl [2.462(1) Å]. Single-crystal X-ray diffraction analysis of a cocrystal of tBuXantphosAuCl and pentafluoronitrobenzene (PFNB) and UV–vis spectroscopic titration experiments revealed the existence of an anion– π interaction between the Cl anion ligand and PFNB. Stoichiometric reaction between PFNB and tBuXantphosAuOtBu, after replacement of Cl by a more nucleophilic tBuO anion ligand, showed higher reactivity and para selectivity in the transformation of C–F to C–OtBu bond, distinctively different from that when only KOtBu was used (ortho selectivity) under the identical condition. Mechanistic studies including density functional theory calculations suggested a gold-mediated nucleophilic ligand attack of the C–F bond pathway via an S_NAr process. On the basis of these results, using trimethylsilyl derivatives TMS–X (X = OMe, SEt, NEt₂) as the nucleophilic ligand source and the fluorine acceptor, catalytic transformation of the C–F bond of aromatic substrates to the C–X (X = O, S, N) bond was achieved with tBuXantphosAuCl as the catalyst (up to 20 turnover numbers).



INTRODUCTION

C–F bond activation attracts increasing attention not only for the importance of fluorinated compounds in pharmaceuticals, agrochemicals, and materials but also for utilization of C–F bonds as organic synthons in organic synthesis.¹ However, the high bond dissociation energy (ca. 140 kcal/mol)² renders C–F bond activation challengeable. Although introducing an “F sink” element such as H,³ B,⁴ Al,⁵ Si,⁶ etc., to form a more stable element–F bond could circumvent the thermodynamic issue,² kinetic issues such as how to lower the activation barrier as well as increase the selectivity still remain to be addressed.⁷ Thanks to the high electronegativity of the F atom, the electrophilic C in the C–F bond is accessible to nucleophilic attack, which had been well documented in organic synthesis.⁸ To enhance the reactivity, selectivity, and functional-group tolerance as well as expand the scope of reactions, metal-catalyzed C–F bond activation has emerged as an important approach along with recent advances in organometallics.^{7,9} Prominently, oxidative addition of the C–F bond has been well exemplified at low-valent transition-metal centers such as Co,¹⁰ Ni,¹¹ Pd,¹² Pt,¹³ or Cu,¹⁴ similar to the C–H bond activation process.^{7,9a,15} Despite tremendous progress made in the last

decades, how to compromise the reactivity and regioselectivity arising from competitive activation of the C–F versus C–H bond (ca. 100 kcal/mol)² became a critical issue.¹⁶

To address this issue, a complementary approach based on the interaction between the ligand on the metal complexes and the C–F bond had been proposed, which combines the advantages of organic transformation and organometallics. Generally, electrophilic or fluorophilic ligand has a tendency to interact with the terminal F of the C–F bond, assisting C–F bond activation, as exemplified by Milsten, Macgregor, Braun, and others.^{4a,17} On the other hand, the nucleophilic ligand (a hydride or an N-, O-, or S-nucleophile) could attack the electrophilic C of the C–F bond, which had been reviewed by Lledos and co-workers in 2011.¹⁸ This would circumvent the problems such as regioselectivity and functional-group tolerance arising from strong organic nucleophiles. However, except for hydrodefluorination (HDF) reactions, most of them were not catalytic but stoichiometric reactions to date. Thus,

Received: November 18, 2015

constructing a catalytic cycle is highly desirable to expand the profile of metal-catalyzed C–F bond transformation.

Our interest in C–F bond activation has prompted us to report the first examples of group 11 metal-catalyzed HDF reactions (copper and gold), which show broad substrate scope, good functional-group tolerance, and high reactivity.¹⁹ To further functionalize the C–F bond, we investigated the reactivity of a nucleophilic ligand besides hydride in gold complexes toward fluoroaromatics. In this work, we found that the ligand strain of the 9,9-dimethyl-4,5-bis(di-*tert*-butylphosphino)xanthene (tBuXantphos) ligand results in an unusually long Au–Cl bond [2.632(1) Å], in which the Cl ligand interacts with a perfluorinated aromatic ring, as shown in the X-ray structure of tBuXantphosAuCl and a pentafluoronitrobenzene (PFNB) cocrystal. Because the Cl ligand is not a good nucleophile and could not react with PFNB, we then replaced Cl[−] with a tBuO[−] ligand and observed the conversion of the *p*-C–F bond to the C–O bond, which has higher reactivity and different regioselectivity compared to those where only KOtBu was used under the same conditions (ortho selectivity). Further experimental and theoretical studies supported a gold(I)-mediated nucleophilic ligand (O or N donors) attack of the C–F bond mechanism. On the basis of these results from stoichiometric reactions, we employed silanes TMS-X (X = OMe, SEt, NEt₂), which provide both “F sink” and nucleophilic ligands, and realized catalytic transformation of C–F to C–X (X = O, S, N) bonds (up to 20 turnover numbers) using tBuXantphosAuCl as the catalyst. These results presented herein highlight the ligand strain of the tBuXantphos ligand on the Au–X bonding and reactivity and also provide an example to design catalytic cycles for C–F transformation based on a gold-mediated S_NAr pathway.

RESULTS AND DISCUSSION

Structure of tBuXantphosAuCl and the Interaction between the Cl Ligand and PFNB. According to our previous work,^{19a} tBuXantphosAuCl exhibited much higher reactivity in HDF reactions than similar tricoordinated XantphosAuCl and bicoordinated gold(I) complexes with either ancillary phosphine or N-heterocyclic carbene (NHC) ligands. To shed light on the ligand effect, we obtained the crystal structure of tBuXantphosAuCl by X-ray diffraction (CCDC 1029200). As shown in Figure 1a, the tricoordination nature of tBuXantphosAuCl is unambiguously shown in its solid structure. Au, P, and Cl atoms lie in the same plane, as indicated by the sum of the P–Au–P, P–Au–Cl, and Cl–Au–P angles [359.7(1)°]. To accommodate this, the tricyclic ring backbone of tBuXantphos is twisted to give a boat conformation. Most strikingly, the Au–Cl bond length in tBuXantphosAuCl is 2.632(1) Å, which is much longer than those in other linear gold(I) complexes supported by PPh₃, NHC, etc., ligands (2.27–2.30 Å)²⁰ and also even longer than that of the similar structure XantphosAuCl [2.462(1) Å].²¹

Interestingly, a weak interaction between tBuXantphosAuCl and PFNB was observed in their UV–vis spectra. Titration of tBuXantphosAuCl to the solution of PFNB in toluene displayed the appearance of a broad, low-energy band centered at ca. 610 nm (Figure 2). This is similar to the charge-transfer band in the solution of (NHC)AuH and PFNB, as we previously reported.^{19b} Upon titration with XantphosAuCl, no low-energy absorption band appeared (Supporting Information, Figure S1). This indicates that weak Au–Cl bonding arising

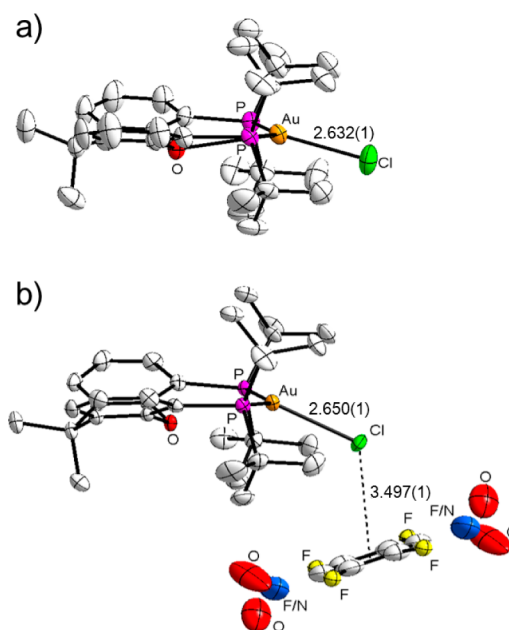


Figure 1. ORTEP diagram of (a) tBuXantphosAuCl and (b) cocrystal of tBuXantphosAuCl/PFNB at the 50% probability. H atoms are omitted for clarity. The nitro group and *p*-F in PFNB are crystallographically disordered.

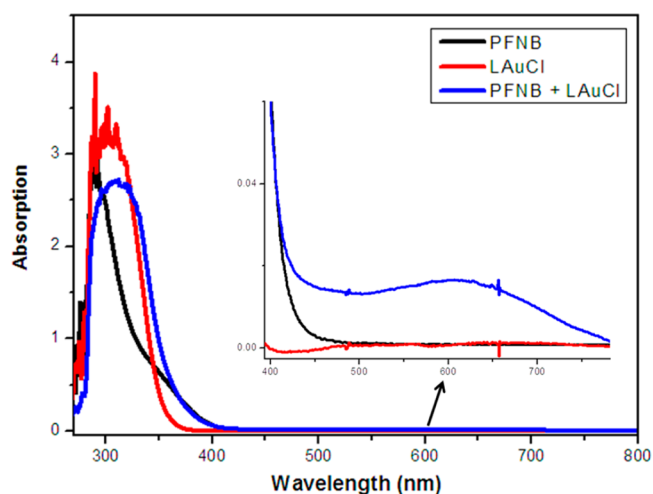


Figure 2. UV–vis absorption spectra of tBuXantphosAuCl (red line), PFNB (black line), and 1:1 tBuXantphosAuCl/PFNB (red line) in a 2 mM toluene solution (the inset shows the charge-transfer band centered at 610 nm).

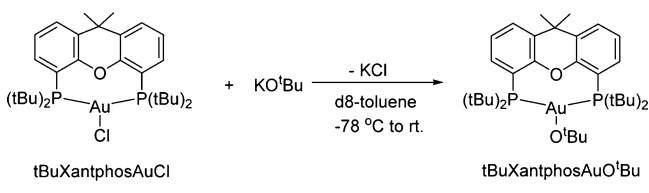
from a long bond distance is important in the interaction between coordinated ligand and C–F bonds.

Slow evaporation of a toluene solution of tBuXantphosAuCl with an excess of PFNB gave a 1:1 tBuXantphosAuCl/PFNB cocrystal (CCDC 1430574). As shown in Figure 1b, the Cl ligand resides above the PFNB ring centroid at a distance of 3.497(1) Å and a 72.6(1)° Cl–centroid axis–ring plane angle. The shortest Cl–C (PFNB) distance [ranging from 3.364(5) to 4.095(4) Å] is 0.09 Å shorter than the sum of their van der Waals radii (3.45 Å). These features have been recognized as indications of anion– π interaction.²² Meanwhile, a slight elongation of the Au–Cl bond [2.632(1) to 2.649(1) Å] also indicated the existence of a possible weak Cl– π interaction. However, refluxing tBuXantphosAuCl and PFNB in toluene did

not afford a C–F bond-activated product, even in the presence of trimethylsilyl chloride (TMS–Cl) as the “F sink”. This might be due to the weak nucleophilicity of the Cl ligand.

Stoichiometric Reactions between LAu–X [X = OtBu and N(iPr)₂] and PFNB. Then we attempted to replace the Cl ligand in tBuXantphosAuCl with a more nucleophilic ligand such as alkoxide. Treatment of tBuXantphosAuCl with KOtBu succeeded in generation of a new gold complex, which we tentatively assigned as tBuXantphosAuOtBu (Scheme 1). The

Scheme 1. Preparation of the tBuXantphosAuOtBu Complex



new compound tBuXantphosAuOtBu shows a singlet at 29.7 ppm in its ³¹P NMR spectrum (Figure 3b), much upfield-shifted compared to that of tBuXantphosAuCl ($\delta_p = 52.8$ ppm; Figure 3a). In the ¹H NMR spectrum, the signal of OtBu appears at 1.63 ppm (Figure S6) and is higher-frequency-shifted than that of KOtBu at 1.09 ppm. Such a chemical shift change was also observed in (IPr)AuOtBu [IPr = *N,N'*-1,3-bis(isopropyl)imidazolin-2-ylidene], which displays a proton signal at 1.23 ppm in toluene-*d*₈.²³ However, this new species was only stable for several hours at ambient temperature and quickly decomposed to gold(0) (dark-purple solution and gold mirror), making it difficult to be fully characterized. Yet the equivalent phosphine nuclei and deshielding of OtBu protons of the complex suggest the tricoordination mode of tBuXantphosAuOtBu shown in Scheme 1.

Thereupon, the reactivity of tBuXantphosAuOtBu toward the C–F bond was investigated. Adding 1 equiv of PFNB in situ prepared tBuXantphosAuOtBu gave *p*- and *o*-(OtBu)-C₆F₄NO₂ in 72% and 10% yield, respectively, after 5 min at room temperature (Figure 3d). Meanwhile, ³¹P NMR spectroscopy evidenced the transformation of tBuXantphosAuOtBu to a new complex showing a singlet at 54.5 ppm (Figure 3c), close to that of tBuXantphosAuCl. The consequent addition of TMS–Cl to the reaction mixture produced TMS–F and tBuXantphosAuCl, which were confirmed by ³¹P and ¹⁹F NMR spectroscopy, respectively (Figure S1). Thus, we

hypothesized that tBuXantphosAuOtBu might convert to a gold fluoride complex, tBuXantphosAuF (Figure 3c), which is the fate of the F atom after C–F bond cleavage. The absence of P–F coupling and a fluorine signal of this “Au–F” compound in the ³¹P and ¹⁹F NMR spectra suggested that the Au–F bond might be of an ionic nature, considering the mismatch of Au⁺ and F[–] according to hard/soft acid–base theory.²⁴ The control experiment of the reaction between KOtBu and PFNB in toluene-*d*₈ gave *p*- and *o*-(OtBu)C₆F₄NO₂ in 4% and 36% yield, respectively. This distinctive reactivity and regioselectivity between tBuXantphosAuOtBu and KOtBu imply that different active intermediates were involved in their reaction with PFNB.

We also noted that a stable and well-characterized gold complex with a nucleophilic ligand has precedence in the literature, such as (IPr)AuOtBu²³ and (IPr)AuN(iPr)₂²⁵ reported by Sadighi and Toste, respectively. Thus, as a comparison and expansion of the nucleophilic ligand, their reactivity was studied as well (Scheme 2). The reaction between (IPr)AuOtBu and PFNB gave *p*- and *o*-(OtBu)-C₆F₄NO₂ in yields of 41% and 22% in 12 h, respectively. (IPr)AuN(iPr)₂ displayed higher reactivity and gave *p*- and *o*-(N(iPr)₂)C₆F₄NO₂ in 54% and 6% yield in 30 min at room temperature, respectively. In both cases, the formation of (IPr)AuF ($\delta_F = -243.2$ ppm) was observed, which precipitated from the reaction mixtures. Thus, the results from stoichiometric reactions unambiguously demonstrated the reactivity of nucleophilic ligands [X = OtBu or N(iPr)₂] of gold complexes supported by either tBuXantphos or NHC ligands toward an aromatic C–F bond.

Mechanistic Studies and DFT Calculations. Several mechanisms for metal-catalyzed C–F bond activation, depending on the different metals, substrates, and reaction conditions, had been proposed and extensively studied.^{7,8b,9a} In this work, to better understand the reactivity of LAu–X toward the C–F bond, we carried out mechanistic studies focusing on three pathways: (1) the oxidative addition of gold(I) to the C–F bond; (2) a radical process; (3) a metal-mediated ligand nucleophilic attack.

The oxidative addition of C–F bonds at low-valent transition metals had been well established.^{3,5c,6–10} However, because of the high redox potential of gold(III)/gold(I) [ca. 1.41 (v)],²⁶ several examples had been recently reported upon the oxidative addition of Si–Si and C–X (X = Br, I) bonds at gold(I).²⁷ To clarify whether gold(I) undergoes oxidative addition of C–F bonds, the Cl-abstracted complex [tBuXantphosAu]⁺[GaCl₄][–]

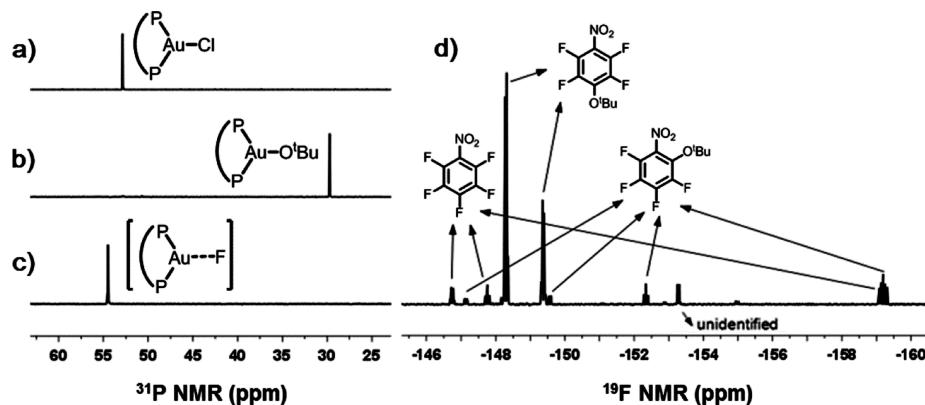
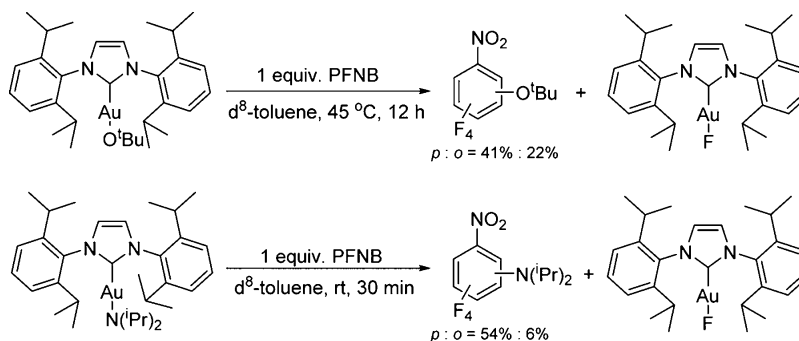
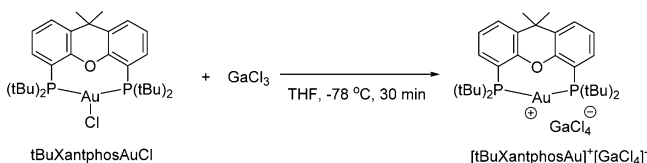


Figure 3. ³¹P NMR spectra: (a) tBuXantphosAuCl; (b) tBuXantphosAuOtBu; (c) upon the addition of 1 equiv of PFNB to tBuXantphosAuOtBu in toluene-*d*₈. (d) ¹⁹F NMR spectrum of the reaction mixture of tBuXantphosAuOtBu with 1 equiv of PFNB.

Scheme 2. Reactions of (IPr)AuX with PFNB [X = OtBu, N(iPr)₂]

was prepared following Bourissou's work (Scheme 3)^{27b} to meet the tetracoordination mode of a possible gold(III) intermediate after the oxidative addition of a C–F bond. The crystal structure is shown in Figure 4, confirming removal of

Scheme 3. Preparation of [tBuXantphosAu]⁺[GaCl₄][−]

intermediate after the oxidative addition of a C–F bond. The crystal structure is shown in Figure 4, confirming removal of

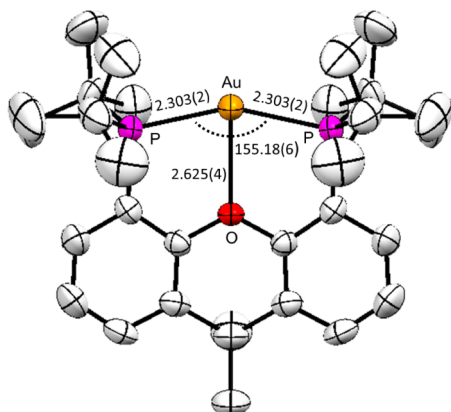


Figure 4. ORTEP diagram of [tBuXantphosAu]⁺[GaCl₄][−] (CCDC 1423270) with 50% ellipsoids. H atoms, solvent molecules, and counterions are omitted for clarity.

the Cl ligand and formation of the noncoordinated [GaCl₄][−] anion (Figure S6). The notable structural changes from this abstraction include (1) expansion of the P–Au–P bond angle from 140.28(4)° to 155.18(6)° and (2) shortening of the Au–O distance from 2.866(3) to 2.625(4) Å, suggesting that the O atom weakly coordinates to the Au atom (Figure 4). However, there is no C–F bond activation found in the reaction between [tBuXantphosAu]⁺[GaCl₄][−] and PFNB, even in refluxing toluene, indicating that [tBuXantphosAu]⁺ could not activate the C–F bond of PFNB. According to our previous calculations,^{19a} the activation energy barrier for C–F bond oxidative addition is high (transition state TS = 30.4 kcal/mol), which is not consistent with our experimental observations. Thus, the oxidative addition–reductive elimination pathway might not be a plausible mechanism.

On the other hand, we added TEMPO to the reaction between tBuXantphosAuOtBu and PFNB and found almost no effect on the reactivity and regioselectivity. Thus, we ruled out one-electron reduction or a radical process mechanism, which had been proposed for some low-valent metals in C–F bond activation.²⁸

A metal-mediated ligand nucleophilic attack of the C–F bond, similar to that of aromatic nucleophilic substitution (S_NAr), had been extensively studied including possible mechanisms.^{11c,e,13a,19,29} In this work, we found that either tBuXantphos- or the NHC-ligand-supported gold(I) *tert*-butyl oxide could activate the C–F bond of PFNB under mild conditions. More importantly, the different nucleophilicities of the coordinated ligand affect the reactivity of the gold complexes [N(iPr)₂ > OtBu > Cl]. In addition, the crystal structures of tBuXantphosAuCl and PFNB clearly suggest the interaction between the coordinated ligand and electrophilic π ring. Thus, we hypothesized that a gold-mediated ligand nucleophilic attack of the C–F bond is the possible mechanism. To estimate the energy profile of the S_NAr reaction pathway, we carried out density functional theory (DFT) studies on the model reaction between tBuXantphosAuOMe (LAu-OMe) and PFNB.³⁰ To make the computation efficient, two methyl groups on the xanthene backbone were replaced by two H atoms, while the bulky tBu groups on phosphine were retained because they were critical for reactivity. Calculations were performed at the DFT (B3LYP)³¹ level with the 6-31G** basis set for the main-group atoms and the SDD³² pseudopotential and associated basis set for the Au atom. The optimized structures of LAu-OMe (Figure 5a) and the final LAu-F (Figure 5b) reserve the tricoordination mode on gold with the Au–O bond as 2.29 Å and the Au–F bond as 2.23 Å.

We focused on the addition–elimination two-step S_NAr process, including the regioselectivity issue, and the calculated reaction profile is depicted in Figure 6. The reaction is initiated by nucleophilic attack at the C–F bond of PFNB with the OMe moiety of LAu-OMe. The corresponding transition state (TS1)

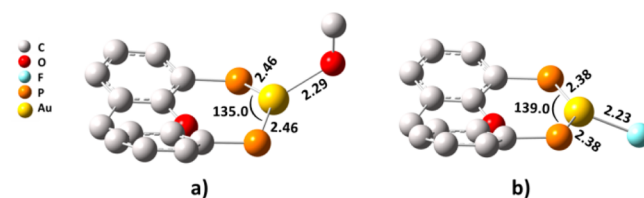


Figure 5. Computed structures of (a) tBuXantphosAuOMe and (b) tBuXantphosAuF with selected bond lengths (Å) and bond angle (deg). H atoms and tBu groups on phosphine are omitted for clarity.

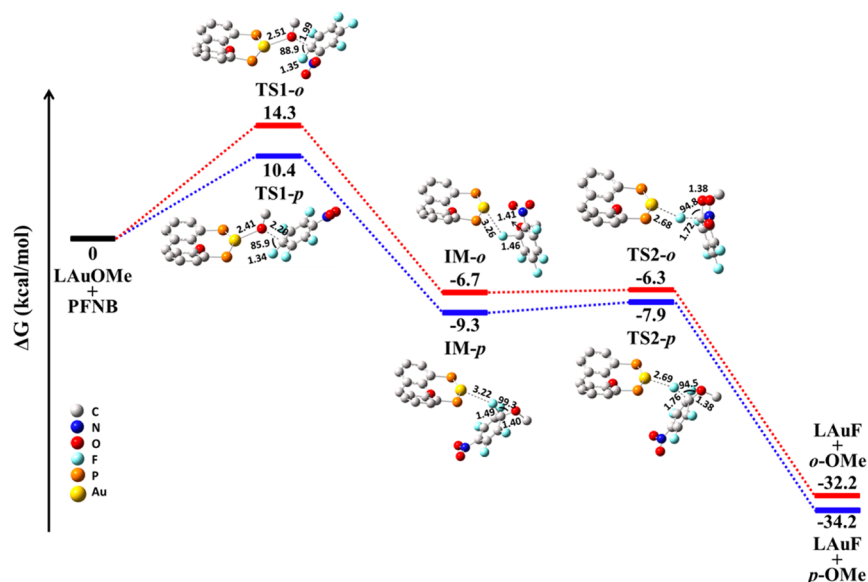
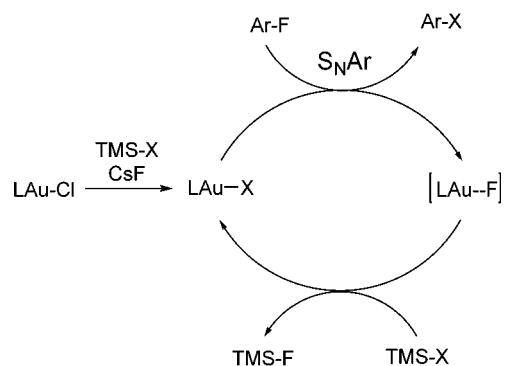


Figure 6. Computed geometries (with selected key distances in angstroms and angles in degrees) and free energy surface for the S_NAr reaction pathway (blue line, para substitution; red line, ortho substitution). H atoms and tBu groups on phosphine are omitted for clarity.

is 10.4 kcal/mol for para attack (TS1-*p*) and 14.3 kcal/mol for ortho attack (TS1-*o*), respectively. In TS1, the OMe group approaches the C center from above the aromatic plane of PFNB, which almost does not affect the corresponding C–F bond length (1.33 Å in PFNB vs 1.34 Å in TS1-*p* and 1.35 Å in TS1-*o*). The Au–O bond is elongated from 2.29 to 2.41 Å in TS1-*p* (2.51 Å in TS1-*o*), and the C–O distance is 2.20 Å in TS1-*p* (1.99 Å in TS1-*o*). The more advanced Au–O bond cleavage and C–O bond formation in TS1-*o* is consistent with its higher energy than that of TS1-*p* (vide infra). The resulting ion-pair intermediates (IM), consisting of a cationic gold complex and an anionic Meisenheimer adduct in short contact, are 9.3 kcal/mol (IM-*p*) and 6.7 kcal/mol (IM-*o*) lower than the starting material. The adducts IM-*o* and IM-*p* share similar structures except for the relative orientation of the cationic gold and the anionic fluorophenyl parts. The C–O bond is substantially shortened to about 1.40 Å, close to 1.33 Å in the final product. The C–F bond is stretched about 0.15–1.49 Å for IM-*p* and 1.46 Å for IM-*o*. The distance between the Au atom and the leaving F atom becomes about 3.2 Å. Next fluoride elimination occurs via TS2, which shows only a subtle structural difference between TS2-*p* and TS2-*o* except for the relative positions of the gold and fluorophenyl moieties, similar to the case of IM2. In TS2-*p*, the C–F bond is further shortened to 1.76 Å (1.72 Å in TS2-*o*) and the Au–O distance is concomitantly reduced to 2.69 Å (2.68 Å in TS2-*o*). The associated energy barrier is 1.4 and 0.4 kcal/mol for TS2-*p* and TS2-*o*, respectively. Overall, the gold-mediated S_NAr pathway for activating either the *p*- or *o*-F atom of PFNB is a highly exothermic process ($\Delta G_p = -34.2$ kcal/mol; $\Delta G_o = -32.2$ kcal/mol). The rate-limiting step is the first step of OMe attacking PFNB, in accordance with the S_NAr mechanism, and has a quite low-energy barrier (<15 kcal/mol). Moreover, attacking the *p*-F atom of PFNB is less energy-demanding than the ortho reaction pathway, which might interpret the observed *p*-F selectivity. In summary, the calculation results are consistent with experimental observations of the reaction of tBuXantphosAuOtBu with PFNB on the selectivity and reactivity.

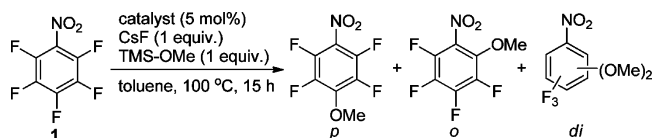
Constructing Catalytic Cycles Based on Stoichiometric Reactions. Encouraged by the results of stoichiometric reactions, we attempted to construct a catalytic cycle based on gold. It is well-known that hydrosilane, often used in HDF reactions, serves as both the “F sink” (Si) and hydrogen source (H) to form fluorosilane and a metal hydride intermediate to activate the C–F bond.^{6b,c,19,33} We thus envisioned that using silanes containing a nucleophile group (X = OR, SR, NR₂, etc.) instead of H might facilitate a catalytic cycle. As shown in Scheme 4, the first step is transmetalation with silanes TMS-X

Scheme 4. Proposed Mechanism of tBuXantphosAuCl-Catalyzed C–F Bond Transformation



to generate a tBuXantphosAuX intermediate. The next step of nucleophilic attack of the C–F bond by tBuXantphosAuX via an S_NAr process gives new C–X bond products and tBuXantphosAuF. Consequent transmetalation of tBuXantphosAuF with silane completes the catalytic cycle with thermodynamically favored Si–F bond formation.

Optimizing Reaction Conditions. As a starting point, we used trimethylmethoxysilane (TMS-OMe) to investigate the transformation of C–F to C–O bond. As shown in Table 1 and Figure 7, tBuXantphosAuCl catalyzed methoxydefluorination of PFNB in good yield (75%) and high para selectivity (*p*:*o*:*di* = 90:5:5, entry 2). The control experiment showed that no reaction occurred in the absence of a metal catalyst or CsF

Table 1. Screening Gold(I) Catalysts^a

entry	catalyst	yield (%) ^b	<i>p</i> : <i>o</i> : <i>di</i> (%) ^b
1	no catalyst or CsF	0	
2	tBuXantphosAuCl	75	90:5:5
3	XantphosAuCl	15	67:27:6
4	(<i>R</i>)-BINAP(AuCl) ₂	0	
5	<i>cis</i> -dppe(AuCl) ₂	0	
6	Xantphos(AuCl) ₂	0	
7	JohnPhosAuCl	0	
8	PCy ₃ AuCl	0	
9	PPh ₃ AuCl	0	
10	(IPr)AuCl	0	
11	(IMes)AuCl	0	
12 ^c	tBuXantphosAuCl	99	90:5:5
13 ^d	tBuXantphosAuCl	23	14:2:2

^aThe reactions were carried out with the catalyst (0.005 mmol), TMS-OMe (0.1 mmol), CsF (0.1 mmol), and PFNB (0.1 mmol) in toluene (2 mL) at 100 °C for 15 h. ^bThe yields and regioselectivity were determined by ¹⁹F NMR spectroscopy versus internal PhCF₃. ^cTMS-OMe (0.2 mmol), 24 h. ^dCatalyst (0.0025 mmol).

(entry 1). XantphosAuCl exhibited moderate reactivity (15%) and decreased selectivity (*p*:*o*:*di* = 67:27:6, entry 3). Other bicoordinated complexes with either ancillary phosphine or NHC ligands had no reactivity (entries 4–11). Increasing the amount of TMS-OMe to 2 equiv and extending the reaction time to 24 h led to full conversion of PFNB without affecting the selectivity (entry 12), while lowering the catalyst loading (2.5 mol %) dramatically reduced the conversion to 23% (entry 13). Solvent effects are shown in Table S1, and toluene is the best solvent. Thus, the optimized conditions tabulated in entry 12 were used for the following investigations.

(IPr)AuCl is inert to catalytic C–F bond activation, whereas (IPr)AuX [X = OtBu and N(iPr)₂] could convert the C–F bond of PFNB to C–O and C–N bonds, respectively. We considered that Au–Cl bonding might be a critical factor of the catalytic performance, which may determine transmetalation of gold chloride to active LAu–X intermediates as we described

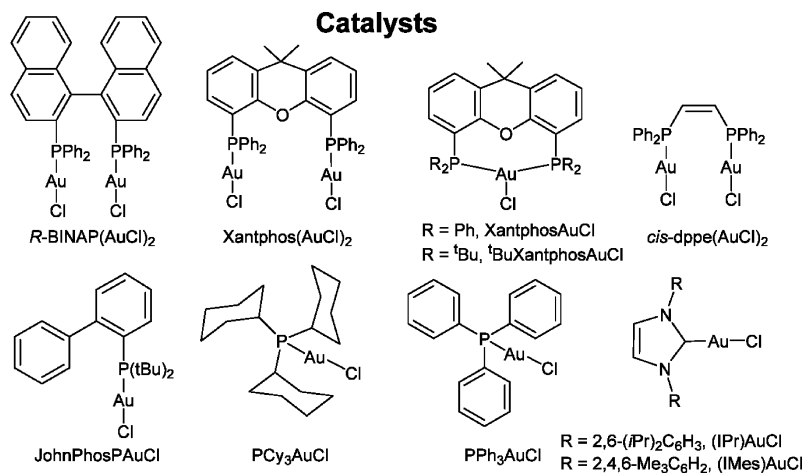
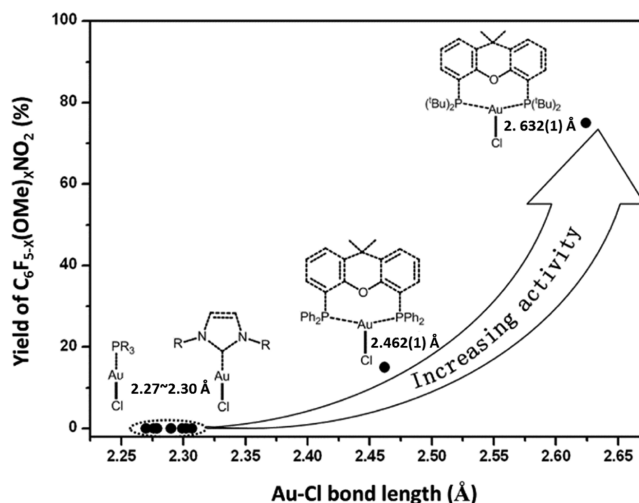


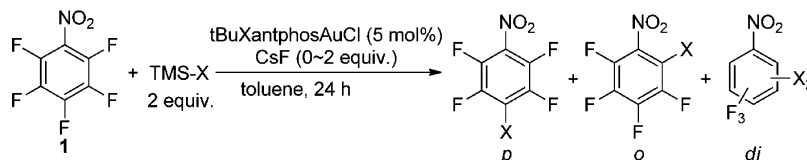
Figure 7. Gold catalysts used in this work.

above. This inference is illustrated in Figure 8, where yields of C₆F_{5-x}(OMe)_xNO₂ versus the Au–Cl bond length^{20,21,34} are

Figure 8. Correlation of the yields of C₆F_{5-x}(OMe)_xNO₂ versus the Au–Cl bond length of the catalysts (*x* = 1, 2).

graphed. It is shown that increasing catalytic performance of the precatalyst LAu–Cl is observed along with elongation of the Au–Cl bond.

Silane Scope. Next, we chose silanes TMS–X containing other nucleophile groups (X = NEt₂, SEt, SiMe₃, Cl) to extend the scope of C–F bond transformation. As shown in Table 2, when TMS–X (X = H, OMe, SEt, NEt₂) was used, the C–F bond of PFNB could be successfully converted to the corresponding C–X bonds nearly quantitatively (entries 2–4 and 6). Notably, C–S bond formation reaction could be achieved at room temperature without adding CsF (entry 3). The reactivity of TMS–X was found to relate to the bond energy (BE) of the Si–X bond.² For example, activating a Si–X bond with higher BE always needs higher CsF loadings and/or higher temperature (entries 3, 4, and 6), following the order of OMe > NEt₂ > SEt. However, other factors, such as steric hindrance of the X group, may also affect the reactivity of Si–X bonds. For example, TMS–SiMe₃ has the lowest BE but no reactivity, which may be due to the steric effect on the formation of an active gold–silyl intermediate (entry 1).

Table 2. Screening of Silanes^a

entry	X	equiv of CsF	temp (°C)	yield (%) ^b	<i>p</i> : <i>o</i> : <i>di</i>	BE of Si–X (kcal/mol) ^c
1	SiMe ₃	2.0	100	0		77.2
2 ^d	H	0	80	>99	73:12:15	95.0
3 ^e	SEt	0	25	>99	100:0:0	99.0
4	NEt ₂	0.5	60	98	92:8:0	108.7
5	Cl	2.0	100	0		115.0
6	OMe	2.0	100	>99	90:5:5	122.6

^aReaction conditions: tBuXantphosAuCl (0.005 mmol), TMS-X (0.2 mmol), PFNB (0.1 mmol), and toluene (2 mL), 24 h unless noted.

^bDetermined by ¹⁹F NMR spectroscopy versus internal PhCF₃. ^cReference 2. ^dReference 19a. ^eSilane 0.12 mmol.

Although TMS-Cl has lower BE than TMS-OMe, no Cl-substituted product was detected because of the inert reactivity of tBuXantphosAuCl toward PFNB.

It is worth noting that direct reactions between PFNB and organic nucleophiles such as NaOMe, NaSiPr, and HNEt₂/NaHCO₃ also afforded the new OMe-, SiPr-, and NEt₂-substituted products but in ortho regioselectivity and lower yields (15–40%), as shown in Table S3. These results clearly revealed the difference between gold-catalyzed C–F transformation and traditional organic methods in reactivity and regioselectivity.

As we proposed, transmetalation of tBuXantphosAuCl with TMS-X (X = OMe, SEt, NEt₂) to active tBuXantphosAuX intermediates is a critical step, which is determined by both Au–Cl and Si–X bonding strength. However, characterization the active tBuXantphosAuX intermediates from transmetalation in situ was not successful. No reaction occurred at room temperature between tBuXantphosAuCl and TMS-X in the presence of CsF, while at elevated temperature (100 °C), decomposition of tBuXantphosAuCl arose (gold mirror and dissociated ligand). This indicates that generated tBuXantphosAuX intermediates are not stable, as we observed in stoichiometric reactions, but could fast react with fluoroaromatics once they were generated.

Substrate Scope. We then extended this protocol to other fluorinated compounds, and the results are shown in Table 3. Generally, TMS-SEt exhibits the highest reactivity and the best functional-group tolerance among the silanes TMS-X (X = OMe, SEt, NEt₂) used, and most transformations of the C–F to C–S bond could be achieved in the absence of CsF at 25 °C. For decreased reactivity of substrates other than PFNB, their reactions with TMS-NEt₂ were conducted at 100 °C.

First, the electronic effect of the substituent on pentafluoroarenes was investigated. Substrates 1 and 2 with strong electron-withdrawing groups (NO₂ and CN) gave products 1a–1c and 2a–2c in high yield (>90%), while 4–6 had no reaction. For 3, the C–S bond formation product 3a could be obtained nearly quantitatively with para selectivity, and no sp³ C–F bond activation was detected.

Functional-group tolerance was examined with pentafluorophenyl derivatives 7–10 containing carboxylate, ester, aldehyde, and ketone groups. The carboxylate moiety is not compatible in this catalytic system, and no C–F activated products were observed for 10. Reactions of 7–9 with TMS-SEt gave the C–S bond formation products 7–9b in ca. 85%

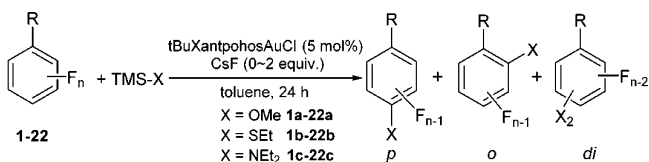
yield, whereas TMS-OMe only exhibited good reactivity toward 7 (75% yield) and no F-substituted product was observed for 8 and 9. In the presence of TMS-NEt₂, only 9 could be converted to 9c in 23% yield, and enol ether CH₂=C(OTMS)(C₆F₅) was produced as a major side product (45%). These results show that the transformation of C–F to C–S bond using TMS-SEt has good functional-group tolerance.

Next, the extent of fluorination of nitrobenzene derivatives (1 and 11–19) was studied. From PFNB to monofluoronitrobenzene, the reactivity of the C–F bond decreases as the fluorine number reduces. No C–F bond activated products were obtained for fluoronitrobenzenes 18 and 19. Interestingly, the extent of fluorination also affects the regioselectivity, showing that less fluorinated substrates tend to undergo *o*-F rather than *p*-F substitution (13, 15, and 17).

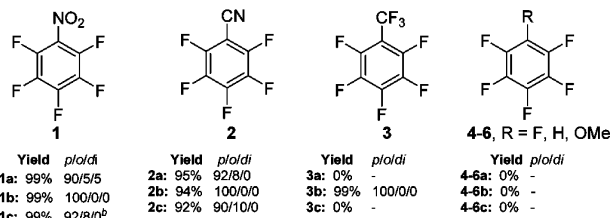
Finally, we examined some heterocyclic and polycyclic compounds 20–22. Pentafluoropyridine 20 is reactive toward all silanes, and the corresponding C–O, C–S, and C–N bond formed products could be obtained in >90% yield with exclusive para selectivity. Compounds 21 and 22 showed moderate reactivity (50–80%) with TMS-OMe and TMS-SEt at 100 °C, but no reactivity with TMS-NEt₂.

CONCLUSIONS

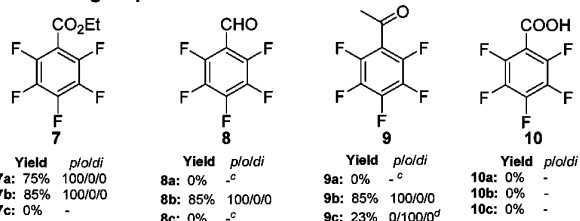
In summary, we describe here the construction a catalytic cycle of C–F to C–X bond (X = O, S, N) transformation based on the gold-mediated ligand-nucleophilic-attack process. The bulky bidentate phosphine ligand tBuXantphos-stabilized tBuXantphosAuCl features an unusually long Au–Cl bond [2.632(1) Å], of which the Cl ligand could interact with the electron-deficient aromatic ring of PFNB but was not able to break the C–F bond. Replacing Cl with the more nucleophilic *tert*-butoxide (tBuO[−]) gave the gold alkoxide complex tBuXantphosAuOtBu, which quickly and selectively converted the *p*-C–F bond of PFNB to a C–O bond. Also, the reactivity was different from that where only KOtBu was used as the nucleophile (lower conversion and ortho selectivity). A similar reactivity was also observed on NHC-supported gold complexes [(IPr)AuOtBu and (IPr)Au(iPr)₂]. Theoretical calculations showed that the S_NAr reaction pathway had a low-energy barrier (<15 kcal/mol) and that *p*-F substitution was less energy-demanding than *o*-F substitution, consistent with our experimental observation. Taking advantage of silane TMS-X (X = OMe, NEt₂, SEt), serving as both a fluorine acceptor and a nucleophilic ligand donor, catalytic C–F bond

Table 3. Substrate Scope^a

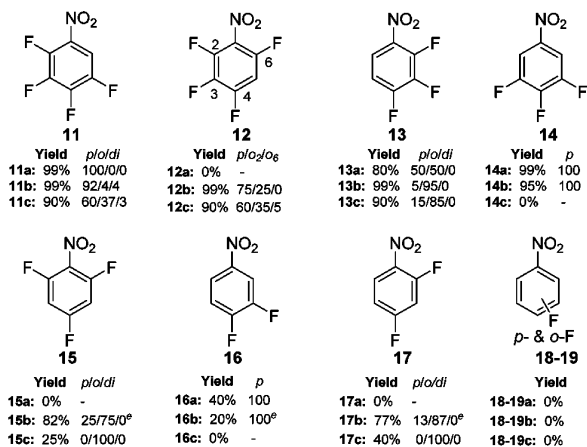
Electronic effect



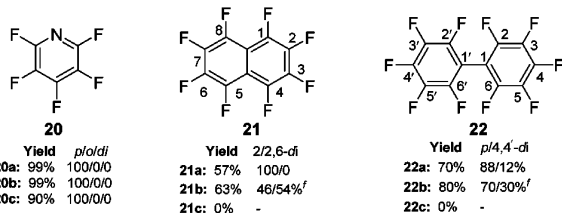
Functional group tolerance



Extent of fluorination



Heterocycle & polycyclic perfluoroarenes



^aReaction conditions: tBuXantphosAuCl (0.005 mmol), substrate (0.1 mmol), TMS-X (0.12–0.2 mmol), CsF (0–0.2 mmol), and toluene (2 mL), 24 h unless noted. For details, see the Supporting Information. ^bCsF (0.05 mmol), 60 °C. ^cMixtures of products. ^dCH₂=C(OTMS)-(C₆F₅) obtained in 45% yield. ^e60 °C. ^f100 °C.

activation thus has been achieved (turnover number of up to 20). These results presented herein provide new access to developing catalytic cycles for C–F bond transformation based on nucleophilic ligand attack of the C–F bond in the coordination sphere.

EXPERIMENTAL SECTION

General Experimental Information. All reactions were performed under an inert atmosphere of argon in either a glovebox or standard Schlenk techniques. 1,2-Dichloroethane was distilled over CaH₂ under nitrogen. Other solvents were purified by a MBRA SPS-800 solvent purification system. Gas chromatography/mass spectrometry (GC/MS) spectra were recorded on a 7890a GC system/5975c mass spectrometer. Electrospray ionization MS spectra were recorded on a Bruker Apex IV Fourier transform ion cyclotron resonance mass spectrometer using electrospray ionization. The intensity data for a crystal of tBuXantphosAuCl were collected on a Bruker Smart Apex II CCD diffractometer with graphite-monochromated Mo K α radiation (0.71073 Å) at 296 K. Crystallographic data for structural analysis of tBuXantphosAuCl, tBuXantphosAuCl/PFNB, and tBuXantphosAu-GaCl₄ are deposited at the Cambridge Crystallographic Data Center as CCDC 1029200, 1430574, and 1423270, respectively. ¹H and ¹⁹F, ¹³C, and ³¹P NMR spectra were recorded on Bruker 400 MHz, Varian 300 MHz, and Bruker 500 MHz instruments at 298 K, respectively. All chemical shifts are reported in ppm, and all coupling constants are in Hz. ¹H NMR spectra are referenced to residual protons (CHCl₃, 7.26 ppm). ¹³C NMR spectra are referenced relative to solvent resonances (CDCl₃, 77.16 ppm). ³¹P{¹H} NMR spectra are referenced to external 85% H₃PO₄ at 0 ppm. ¹⁹F NMR spectra are referenced to external CF₃COOH at –78.5 ppm (for the mechanism study) or 0 ppm (for products).

Synthesis and Reactivity of tBuXantphosAuOtBu (in Situ NMR). In a glovebox, tBuXantphosAuCl (7.3 mg, 0.01 mmol) was dissolved in 0.4 mL of toluene-*d*₈ in an NMR tube sealed with a rubber cap. KOTu (1.2 mg, 0.01 mmol) was dissolved in 0.3 mL of toluene-*d*₈ and then transferred to a syringe equipped with stainless steel needles. The syringe was closed by blocking the needles with a septum. Outside the glovebox, the tBuXantphosAuCl solution was precooled to –78 °C, and then the KOTu solution was added via syringe slowly with shaking of the NMR tube to ensure mixing. After the addition was complete, the NMR tube was allowed to warm to room temperature freely, giving a light-yellow solution. Then PFNB (1.3 μ L, 0.01 mmol) was added via syringe to the above solution. Upon shaking of the NMR tube to ensure mixing, the sample was directly used for NMR analysis.

Reaction of (IPr)AuOtBu with PFNB. In a glovebox, (IPr)-AuOtBu (10 mg, 0.015 mmol) was placed in a Wilmad low-pressure/vacuum NMR tube, and then 0.6 mL of toluene-*d*₈ was added. After almost the entire complex was dissolved, PFNB (2 μ L, 0.015 mmol) was added into the solution. Then the NMR tube was sealed, taken out, covered with aluminum foil, and placed into a 45 °C oil bath. The reaction process was monitored by ¹⁹F NMR. As the reaction proceeded, a white solid precipitated slowly. After the reaction was complete, the white solid was collected, dried, and characterized by NMR. Its characteristic ¹⁹F NMR signal at –257 ppm in CD₂Cl₂ and its ¹H NMR spectrum confirmed it to be the known (IPr)AuF.²³ The reaction of (IPr)AuN(iPr)₂ with PFNB was carried out similarly.

Computational Method. All calculations were carried out with the Gaussian 09 package.³⁰ All molecular geometries were optimized at the DFT (B3LYP)³¹ level with the 6-31G** basis set for the main-group atoms and the SDD³² pseudopotential and associated basis set for the Au atom. The frequency calculations at the same level were carried out to confirm each stationary point to be either a minimum or a transition state. Intrinsic reaction coordinate paths were calculated to connect each TS to the corresponding reactant and product. The solvent effect (toluene) was incorporated via a polarized continuum model³⁵ based on gas-phase-optimized geometries. To make computations efficient, the two methyl groups on the xanthene backbone were replaced by two H atoms.

Catalytic C–F Bond Transformation. In a glovebox, into a 25 mL Schlenk tube was placed tBuXantphosAuCl (3.7 mg, 0.005 mmol), CsF (30.4 mg, 0.2 mmol), and 2 mL of toluene. Then TMS-OMe (28 μ L, 0.2 mmol) and PFNB (13 μ L, 0.1 mmol) was added to the tube, and the tube was heated to 100 °C for 24 h. When the reaction was complete, a small portion of the reaction mixture (~0.2 mL) was taken

from the Schlenk tube and passed through a short column of silica gel with DCM as the eluent to give the sample for GC/MS analysis. Another 0.5 mL of the reaction mixture was directly added into a NMR tube for NMR analysis, and the yields of the products were determined by integration in the ^{19}F NMR spectrum versus internal PhCF_3 . For C–N bond formation, 0.2 mmol of TMS-NEt_2 and 0.2 mmol of CsF were used and the reaction temperature was 100 °C (except for that of PFNB). For C–S bond formation, 0.12 mmol of TMS-SEt was used and the typical temperature was 25 °C.

■ ASSOCIATED CONTENT

● Supporting Information

The Supporting Information is available free of charge on the ACS Publications website at DOI: 10.1021/acs.inorgchem.5b02634.

Detailed experimental procedures and characterization of new compounds, crystallographic data, and coordinates of the DFT-optimized intermediates and transition states (PDF)

CIF file (CIF)

CIF file (CIF)

CIF file (CIF)

■ AUTHOR INFORMATION

Corresponding Authors

*E-mail: haolingsun@bnu.edu.cn.

*E-mail: zhangjunlong@pku.edu.cn.

Notes

The authors declare no competing financial interest.

■ ACKNOWLEDGMENTS

This project was supported by the National Key Basic Research Support Foundation of China (Grants 2010CB912302 and 2015CB856301) and National Scientific Foundation of China (Grants 20971007, 21571007, 21271013, 21321001, and 21101169).

■ REFERENCES

- (1) (a) Hiyama, T.; Yamamoto, H. *Organofluorine compounds: chemistry and applications*; Springer: Berlin, 2000. (b) Kirsch, P.; *Modern Fluoroorganic Chemistry: Synthesis, Reactivity, Applications*, Wiley-VCH Verlag GmbH & Co. KGaA: Weinheim, Germany, 2004. (c) Uneyama, K. *Organofluorine chemistry*; John Wiley & Sons: New York, 2008. (d) Kirk, K. L. *Org. Process Res. Dev.* **2008**, *12*, 305.
- (2) Luo, Y.-R. *Comprehensive handbook of chemical bond energies*; CRC Press: Boca Raton, FL, 2010.
- (3) (a) Aizenberg, M.; Milstein, D. *J. Am. Chem. Soc.* **1995**, *117*, 8674. (b) Noveski, D.; Braun, T.; Neumann, B.; Stammer, A.; Stammer, H.-G. *Dalton Trans.* **2004**, 4106. (c) Braun, T.; Noveski, D.; Ahijado, M.; Wehmeier, F. *Dalton Trans.* **2007**, 3820.
- (4) (a) Teltewskoi, M.; Panetier, J. A.; Macgregor, S. A.; Braun, T. *Angew. Chem., Int. Ed.* **2010**, *49*, 3947. (b) Källäne, S. I.; Teltewskoi, M.; Braun, T.; Braun, B. *Organometallics* **2015**, *34*, 1156.
- (5) (a) Jäger-Fiedler, U.; Klahn, M.; Arndt, P.; Baumann, W.; Spannenberg, A.; Burlakov, V. V.; Rosenthal, U. *J. Mol. Catal. A: Chem.* **2007**, *261*, 184. (b) Yow, S.; Gates, S. J.; White, A. J.; Crimmin, M. R. *Angew. Chem.* **2012**, *124*, 12727.
- (6) (a) Aizenberg, M.; Milstein, D. *Science* **1994**, *265*, 359. (b) Vela, J.; Smith, J. M.; Yu, Y.; Ketterer, N. A.; Flaschenriem, C. J.; Lachicotte, R. J.; Holland, P. L. *J. Am. Chem. Soc.* **2005**, *127*, 7857. (c) Kühnel, M. F.; Lentz, D. *Angew. Chem., Int. Ed.* **2010**, *49*, 2933.
- (7) Kühnel, M. F.; Lentz, D.; Braun, T. *Angew. Chem., Int. Ed.* **2013**, *52*, 3328.
- (8) (a) Brooke, G. M. *J. Fluorine Chem.* **1997**, *86*, 1. (b) Amii, H.; Uneyama, K. *Chem. Rev.* **2009**, *109*, 2119.
- (9) (a) Perutz, R. N.; Braun, T. In *Comprehensive Organometallic Chemistry III*; Crabtree, D. M. P. M. H., Ed.; Elsevier: Oxford, U.K., 2007; p 725. (b) Whittlesey, M. K.; Peris, E. *ACS Catal.* **2014**, *4*, 3152. (c) Weaver, J.; Senaweera, S. *Tetrahedron* **2014**, *70*, 7413. (d) Ahrens, T.; Kohlmann, J.; Ahrens, M.; Braun, T. *Chem. Rev.* **2015**, *115*, 931. (e) Hu, J.-Y.; Zhang, J.-L. In *Organometallic Fluorine Chemistry*; Braun, T., Hughes, R. P., Eds.; Springer International Publishing: Cham, Switzerland, 2015; Vol. 52, p 143.
- (10) (a) Li, X.; Sun, H.; Yu, F.; Flörke, U.; Klein, H.-F. *Organometallics* **2006**, *25*, 4695. (b) Camadanli, S.; Beck, R.; Flörke, U.; Klein, H.-F. *Dalton Trans.* **2008**, 5701. (c) Dugan, T. R.; Goldberg, J. M.; Brennessel, W. W.; Holland, P. L. *Organometallics* **2012**, *31*, 1349. (d) Li, J.; Zheng, T.; Sun, H.; Xu, W.; Li, X. *Dalton Trans.* **2013**, 42, 5740.
- (11) (a) Fahey, D. R.; Mahan, J. E. *J. Am. Chem. Soc.* **1977**, *99*, 2501. (b) Sladek, M. I.; Braun, T.; Neumann, B.; Stammer, H.-G. *J. Chem. Soc., Dalton Trans.* **2002**, 297. (c) Schaub, T.; Fischer, P.; Steffen, A.; Braun, T.; Radius, U.; Mix, A. *J. Am. Chem. Soc.* **2008**, *130*, 9304. (d) Johnson, S. A.; Taylor, E. T.; Cruise, S. J. *Organometallics* **2009**, *28*, 3842. (e) Johnson, S. A.; Mroz, N. M.; Valdizon, R.; Murray, S. *Organometallics* **2011**, *30*, 441. (f) Breyer, D.; Berger, J.; Braun, T.; Mebs, S. *J. Fluorine Chem.* **2012**, *143*, 263.
- (12) (a) Jasim, N. A.; Perutz, R. N.; Whitwood, A. C.; Braun, T.; Izundu, J.; Neumann, B.; Rothfeld, S.; Stammer, H.-G. *Organometallics* **2004**, *23*, 6140. (b) Braun, T.; Izundu, J.; Steffen, A.; Neumann, B.; Stammer, H.-G. *Dalton Trans.* **2006**, 5118. (c) Breyer, D.; Braun, T.; Kläring, P. *Organometallics* **2012**, *31*, 1417.
- (13) (a) Hofmann, P.; Unfried, G. *Chem. Ber.* **1992**, *125*, 659. (b) Crespo, M.; Martinez, M.; Sales, J. *Organometallics* **1993**, *12*, 4297. (c) Crespo, M.; Solans, X.; Font-Bardia, M. *Organometallics* **1995**, *14*, 355. (d) Wang, T.; Alfonso, B. J.; Love, J. A. *Org. Lett.* **2007**, *9*, 5629. (e) Nova, A.; Erhardt, S.; Jasim, N. A.; Perutz, R. N.; Macgregor, S. A.; McGrady, J. E.; Whitwood, A. C. *J. Am. Chem. Soc.* **2008**, *130*, 15499. (f) Buckley, H. L.; Wang, T.; Tran, O.; Love, J. A. *Organometallics* **2009**, *28*, 2356.
- (14) Casitas, A.; Canta, M.; Sola, M.; Costas, M.; Ribas, X. *J. Am. Chem. Soc.* **2011**, *133*, 19386.
- (15) Osterberg, C. E.; Richmond, T. G. *ACS Symposium Series*; American Chemical Society: Washington, DC, 1994; Vol. 555, p 392.
- (16) Clot, E.; Eisenstein, O.; Jasim, N.; Macgregor, S. A.; McGrady, J. E.; Perutz, R. N. *Acc. Chem. Res.* **2011**, *44*, 333.
- (17) (a) Blum, O.; Frolov, F.; Milstein, D. *J. Chem. Soc., Chem. Commun.* **1991**, 258. (b) Jasim, N. A.; Perutz, R. N.; Whitwood, A. C.; Braun, T.; Izundu, J.; Neumann, B.; Rothfeld, S.; Stammer, H.-G. *Organometallics* **2004**, *23*, 6140. (c) Macgregor, S. A.; Roe, D. C.; Marshall, W. J.; Bloch, K. M.; Bakhmutov, V. I.; Grushin, V. V. *J. Am. Chem. Soc.* **2005**, *127*, 15304. (d) Macgregor, S. A. *Chem. Soc. Rev.* **2007**, *36*, 67. (e) Erhardt, S.; Macgregor, S. A. *J. Am. Chem. Soc.* **2008**, *130*, 15490. (f) Nova, A.; Reinhold, M.; Perutz, R. N.; Macgregor, S. A.; McGrady, J. E. *Organometallics* **2010**, *29*, 1824. (g) Raza, A. L.; Panetier, J. A.; Teltewskoi, M.; Macgregor, S. A.; Braun, T. *Organometallics* **2013**, *32*, 3795.
- (18) Nova, A.; Mas-Balleste, R.; Lledos, A. *Organometallics* **2012**, *31*, 1245.
- (19) (a) Zhan, J. H.; Lv, H.; Yu, Y.; Zhang, J. L. *Adv. Synth. Catal.* **2012**, *354*, 1529. (b) Lv, H.; Zhan, J.-H.; Cai, Y.-B.; Yu, Y.; Wang, B.; Zhang, J.-L. *J. Am. Chem. Soc.* **2012**, *134*, 16216. (c) Lv, H.; Cai, Y. B.; Zhang, J. L. *Angew. Chem.* **2013**, *125*, 3285.
- (20) (a) Baenziger, N. C.; Bennett, W. E.; Soborofe, D. M. *Acta Crystallogr., Sect. B: Struct. Crystallogr. Cryst. Chem.* **1976**, *32*, 962. (b) de Frémont, P.; Scott, N. M.; Stevens, E. D.; Nolan, S. P. *Organometallics* **2005**, *24*, 2411.
- (21) Ito, H.; Saito, T.; Miyahara, T.; Zhong, C. M.; Sawamura, M. *Organometallics* **2009**, *28*, 4829.
- (22) (a) Mooibroek, T. J.; Black, C. A.; Gamez, P.; Reedijk, J. *Cryst. Growth Des.* **2008**, *8*, 1082. (b) Frontera, A.; Gamez, P.; Mascal, M.; Mooibroek, T. J.; Reedijk, J. *Angew. Chem., Int. Ed.* **2011**, *50*, 9564. (c) Chifotides, H. T.; Dunbar, K. R. *Acc. Chem. Res.* **2013**, *46*, 894.

- (23) Laitar, D. S.; Müller, P.; Gray, T. G.; Sadighi, J. P. *Organometallics* **2005**, *24*, 4503.
- (24) Pearson, R. G. *J. Am. Chem. Soc.* **1963**, *85*, 3533.
- (25) Johnson, M. W.; Shevick, S. L.; Toste, F. D.; Bergman, R. G. *Chem. Sci.* **2013**, *4*, 1023.
- (26) Bratsch, S. G. *J. Phys. Chem. Ref. Data* **1989**, *18*, 1.
- (27) (a) Gualco, P.; Ladeira, S.; Miqueu, K.; Amgoune, A.; Bourissou, D. *Angew. Chem., Int. Ed.* **2011**, *50*, 8320. (b) Joost, M.; Zeineddine, A.; Estévez, L.; Mallet-Ladeira, S.; Miqueu, K.; Amgoune, A.; Bourissou, D. *J. Am. Chem. Soc.* **2014**, *136*, 14654. (c) Guenther, J.; Mallet-Ladeira, S.; Estevez, L.; Miqueu, K.; Amgoune, A.; Bourissou, D. *J. Am. Chem. Soc.* **2014**, *136*, 1778. (d) Joost, M.; Gualco, P.; Coppel, Y.; Miqueu, K.; Kefalidis, C. E.; Maron, L.; Amgoune, A.; Bourissou, D. *Angew. Chem., Int. Ed.* **2014**, *53*, 747.
- (28) (a) Hintermann, S.; Pregosin, P. S.; Rügger, H.; Clark, H. C. *J. Organomet. Chem.* **1992**, *435*, 225. (b) Whittlesey, M. K.; Perutz, R. N.; Moore, M. H. *Chem. Commun.* **1996**, 787. (c) Whittlesey, M. K.; Perutz, R. N.; Greener, B.; Moore, M. H. *Chem. Commun.* **1997**, 187.
- (29) (a) Park, S.; Pontier-Johnson, M.; Roundhill, D. M. *J. Am. Chem. Soc.* **1989**, *111*, 3101. (b) Cochran, F. V.; Bonitatebus, P. J.; Schrock, R. R. *Organometallics* **2000**, *19*, 2414. (c) Deck, P. A.; Konaté, M. M.; Kelly, B. V.; Slobodnick, C. *Organometallics* **2004**, *23*, 1089. (d) Nova, A.; Mas-Balleste, R.; Ujaque, G.; Gonzalez-Duarte, P.; Lledos, A. *Chem. Commun.* **2008**, 3130. (e) Nova, A.; Mas-Balleste, R.; Ujaque, G.; Gonzalez-Duarte, P.; Lledos, A. *Dalton Trans.* **2009**, 5980. (f) Scharf, A.; Goldberg, I.; Vigalok, A. *Organometallics* **2012**, *31*, 1275.
- (30) Frisch, M. J.; et al. *Gaussian 09*; Gaussian, Inc.: Wallingford, CT, 2009.
- (31) (a) Lee, C.; Yang, W.; Parr, R. G. *Phys. Rev. B: Condens. Matter Mater. Phys.* **1988**, *37*, 785. (b) Becke, A. D. *J. Chem. Phys.* **1993**, *98*, 5648.
- (32) Andrae, D.; Haeussermann, U.; Dolg, M.; Stoll, H.; Preuss, H. *Theor. Chim. Acta* **1990**, *77*, 123.
- (33) (a) Beltrán, T. F.; Feliz, M.; Llusar, R.; Mata, J. A.; Safont, V. S. *Organometallics* **2011**, *30*, 290. (b) Kuehnle, M. F.; Holstein, P.; Kliche, M.; Krüger, J.; Matthies, S.; Nitsch, D.; Schutt, J.; Sparenberg, M.; Lentz, D. *Chem. - Eur. J.* **2012**, *18*, 10701. (c) Fischer, P.; Götz, K.; Eichhorn, A.; Radius, U. *Organometallics* **2012**, *31*, 1374. (d) Zámstná, L.; Ahrens, M.; Braun, T. *J. Fluorine Chem.* **2013**, *155*, 132.
- (34) (a) Jones, P. G. *Acta Crystallogr., Sect. B: Struct. Crystallogr. Cryst. Chem.* **1980**, *36*, 2775. (b) Muir, J. A.; Muir, M. M.; Pulgar, L. B.; Jones, P. G.; Sheldrick, G. M. *Acta Crystallogr., Sect. C: Cryst. Struct. Commun.* **1985**, *41*, 1174. (c) Pintado-Alba, A.; de la Riva, H.; Nieuwhuyzen, M.; Bautista, D.; Raithby, P. R.; Sparkes, H. A.; Teat, S. J.; Lopez-de-Luzuriaga, J. M.; Lagunas, M. C. *Dalton Trans.* **2004**, 3459. (d) Fructos, M. R.; Belderrain, T. R.; de Frémont, P.; Scott, N. M.; Nolan, S. P.; Díaz-Requejo, M. M.; Pérez, P. *J. Angew. Chem., Int. Ed.* **2005**, *44*, 5284. (e) Herrero-Gómez, E.; Nieto-Oberhuber, C.; López, S.; Benet-Buchholz, J.; Echavarren, A. M. *Angew. Chem., Int. Ed.* **2006**, *45*, 5455. (f) Bats, J. W.; Hamzic, M.; Hashmi, A. S. K. *Acta Crystallogr., Sect. E: Struct. Rep. Online* **2007**, *63*, m2344.
- (35) (a) Tomasi, J.; Persico, M. *Chem. Rev.* **1994**, *94*, 2027. (b) Cossi, M.; Scalmani, G.; Rega, N.; Barone, V. *J. Chem. Phys.* **2002**, *117*, 43. (c) Tomasi, J.; Mennucci, B.; Cammi, R. *Chem. Rev.* **2005**, *105*, 2999.